JOURNAL OF MECHANICAL ENGINEERING AND SCIENCES
ISSN: 2289-4659 e-ISSN: 2231-8380
VOLUME 19, ISSUE 4, 2025, 10908 - 10922
DOI: https://doi.org/10.15282/jmes.19.4.2025.7.0855

RESEARCH ARTICLE

# Computational analysis of hemodynamic parameters in coronary arteries: Effects of stenosis and bifurcation angle

**S. H. Maowa[1], M. Masum Billah[1], K. E. Hoque[1]*, N. F. Ifraj[1], M. S. Hossain[1], S. M. A Hoq[2]**

[1] Department of Arts and Sciences, Faculty of Engineering, Ahsanullah University of Science and Technology, 141 & 142, Love Road, Tejgaon Industrial Area, Dhaka-1208, Bangladesh
[2] Department of Science in Engineering, Faculty of Engineering, International Islamic University Malaysia, P.O. Box 10, 50728 Kuala Lumpur, Malaysia

**ABSTRACT -** Cardiovascular diseases (CVDs) are still becoming the number one cause of death around the world. Coronary artery disease (CAD) is one of the most prevalent types. It is exceedingly crucial to monitor hemodynamic parameters early and precisely in order to determine progresses to become more severe, particularly in regions where arteries bifurcated. This study employs computational fluid dynamics (CFD) simulations to investigate how stenosis and bifurcation angle influence blood flow in the coronary arteries. Seven idealized 3D models of coronary arteries have been developed to show various degrees of narrowing in the arteries. The Carreau model was used to model blood as a non-Newtonian fluid, and the Navier-Stokes equations were used to perform simulations across the cardiac cycle. Key hemodynamic variables like velocity, pressure, and wall shear stress (WSS) were extracted. Results demonstrate that areas with 85% stenosis had maximum velocity of 3.52 m/s, wall shear stress of 78 Pa, and pressures of up to 230 mmHg at time t = 0.63 s. These are high-risk areas for disease progression. These outcomes assist in understanding how the shape of arteries affects abnormal flow dynamics, which could help medical professionals find and treat CAD early on.

**ARTICLE HISTORY**
Received : 4th Mar. 2025
Revised : 22nd Oct. 2025
Accepted : 22nd Oct. 2025
Published : 29th Dec. 2025

**KEYWORDS**
*CVDs*
*Coronary artery bifurcation*
*CFD*
*Stenosis*
*Hemodynamic parameters*

## 1. INTRODUCTION

Cardiovascular diseases (CVDs) have grown much more common in recent years, and they are now a major cause of death and disability around the world. Coronary artery disease (CAD) is one of the most life-threatening CVDs and needs new ways to diagnose and treat it [1]. The development of CAD is very complex and depends on the blood flow characteristics and artery geometries of each patient. A better understanding of how blood flows, particularly at arterial bifurcations, may help make diagnoses more precise. Recent computational investigations into coronary artery hemodynamics have shed light on how stenosis and bifurcation angle critically shape flow patterns and wall shear stress. Studies employing CFD have consistently shown that even minor variations in bifurcation geometry can lead to significant changes in local hemodynamics, which may influence plaque formation and progression [2–4]. More recently, machine learning approaches have complemented these simulations, allowing for rapid and patient-specific predictions without sacrificing accuracy [2, 5]. A hybrid modelling framework combining computational fluid dynamics, fluid–structure interaction, and physics-informed neural networks was later proposed to improve the prediction of fractional flow reserve in stenotic coronary trees [6].

Analyses focusing on patient-derived anatomies have highlighted that flow disturbances caused by stenosis severity and branching angles are highly individualized, emphasizing the need for personalized assessment [7–9]. In addition, combining CFD with non-invasive imaging and deep learning has demonstrated the potential to predict coronary occlusion risk effectively, providing a bridge between computational modeling and clinical decision-making [10, 11]. Patient-specific simulations further highlighted how stent deployment in realistic bifurcation geometries can significantly alter local hemodynamics [12], while comparative investigations of different two-stent techniques across multiple bifurcation angles revealed that certain strategies increased restenosis risk through unfavourable shear profiles [13]. Insights from simulations of bypass grafting further reinforce the impact of stenosis location and severity on postoperative flow dynamics and graft performance [14]. Collectively, these works illustrate that integrating computational modeling with modern data-driven tools offers a nuanced understanding of coronary artery hemodynamics, paving the way for better-informed intervention strategies [15]. Finally, pre-procedural planning research demonstrated that CCTA-guided bifurcation PCI using FFR_CT virtual PCI and myocardial mass evaluation can significantly improve planning and clinical outcomes [16].

In the past few decades, scientists have achieved a lot of progress in understanding how hemodynamic variables impact the development of coronary artery disease. Numerous investigations have examined computational hemodynamics in the context of coronary artery bifurcations, which have helped to clarify the complicated flow patterns and hemodynamic conditions that occur with different bifurcation angles and levels of stenosis. For complex shapes, a

*CORRESPONDING AUTHOR | K. E. Hoque | ekram_math.as@aust.edu

hybrid discretization method that used both tetrahedral and hexahedral elements was used to get precise outcomes. Rabbi *et al.* [17] examined more than one anatomical scenario and showed how geometric factors like branch angle and tortuosity impact left coronary artery hemodynamics and the development of atherosclerosis. Building on these findings, recent studies have offered valuable insights into how bifurcation geometry and stenosis shape blood flow. For example, Bouteloup *et al.* [18] showed that pre-bifurcation stenosis can significantly change hemodynamics in carotid arteries, a pattern that closely mirrors what happens in coronary vessels. Mohd Adib *et al.* [19] highlighted the power of combining MRI and CFD for patient-specific bifurcation analysis—a technique that is increasingly being applied to coronary arteries. Similarly, Nayak *et al.* [20] examined flow in aneurysmal geometries and found that small variations in vessel shape can strongly influence wall shear stress, echoing findings in stenotic bifurcations. Belaghit *et al.* [21] demonstrated how stent placement can reshape local pressure and shear patterns throughout the cardiac cycle. More recent work has also emphasized the role of realistic blood properties, such as non-Newtonian behavior, in accurately capturing arterial flow [22]. Altogether, these studies reinforce a key point: computational modeling provides a powerful lens for understanding the complex interaction between stenosis, vessel geometry, and hemodynamics.

Researchers have extensively investigated how different bifurcation angles affected blood flow in the left coronary bifurcation [23]. Their CFD simulations showed that the maximum velocity of flow was influenced by the bifurcation angle and the flow stability. The study [24] looked at stenting in coronary bifurcations and found that the patterns of stenosis were different before and after stenting. Prior studies [25] explored blood rheology and platelet activity across a narrowed coronary bifurcation and stressed how important it is to have accurate multiphase models capable of capture non-Newtonian effects and predict atherosclerotic tendencies.

Subsequent investigations [26] investigated how stenosis and arterial shape interact to affect blood flow in narrowed arteries. Researchers [27] found that the peak velocity of blood flow in atherosclerotic human arteries was dependent on the geometry and height of the stenosis. Related studies [28] illustrated the impact of coronary bifurcation angle upon computed tomography-derived fractional flow capacity for coronary vessels free of evident coronary artery disease. Flow analysis of blood through a bifurcated and narrowed coronary artery was studied [29]. Two models where one healthy and one idealized for a particular patient, were taken into account for this research. The relationship between bifurcation angles and CAD has been investigated. When examining hemodynamic parameters in 80% of stenosis cases, [30] found that plaque buildup happened when the pressure drop and shear stress at larger bifurcation angles improved.

The authors [31] examined the precision of CT angiography is at finding bifurcation angles and found that there was significant variance in real-life situations. Other investigations [32] used coronary CT angiography data to investigate how bifurcation angles affect the risk factors for coronary heart disease. Also, both [33] and [34] examined how flow and endothelial function change in bifurcated coronary arteries. Dhungana *et al.* [35] investigated into how the bifurcation angle influenced blood flow and wall shear stress. They found that bigger angles caused more recirculation and a bigger pressure gradient. Several studies [36] looked into how geometric factors affect coronary blood flow by making two-dimensional (2D) and three-dimensional (3D) models of the human left coronary artery in both normal and stenotic conditions. They observed that a 2D model was good enough for measuring blood flow in healthy people, but a 3D model was needed to measure blood flow in sick people, especially those with 80% stenosis.

Many studies examined at stenosis because it is common in people with coronary artery disease. Jahangiri *et al.* [37] performed a numerical study of pulsatile blood flow in elastic arteries with one or more stenoses to find out how stenoses change the way blood flows. The research found that as the number of stenoses grew, the flow patterns in the narrowed areas changed. There was a clear change in the oscillatory zones behind each stenosis. A physics-based model for rapid blood flow and pressure prediction was developed by [38], which would allow for calculations such as the fractional flow reserve from coronary computed CT angiography. This could be used for determining the location of tissue death caused by a lesion. The flow dynamics in tortuous coronary arteries with symmetric and asymmetric stenosis were also investigated by [39, 40] who found that time-averaged wall shear stress (TAWSS) may be useful in detecting disease hotspots. Prior work [41] investigated turbulent blood flow in flexible arteries with single and double stenosis. The study revealed noticeable differences in flow patterns, pressure drops, and wall shear stress between the two stenosis conditions. The authors [42] studied non-Newtonian blood flow at a femoral artery bifurcation with mild arteriosclerosis to better understand flow behavior in impaired arterial systems. A recent study has examined how bifurcation angles affect coronary hemodynamics. Recent studies [43] simulated blood flow in bifurcated coronary arteries with different angles, showing recirculation rate and pressure gradient changes. Further studies [44] found the best stent placement for reducing neointimal hyperplasia in pulsatile flow stented bifurcation coronary arteries. In one of the most recent studies, [45] studied the role of bifurcation angles in shaping blood flow patterns within stenotic arteries of the left coronary artery. The findings highlight how arterial geometry affects recirculation, wall shear stress (WSS), and oscillatory shear index (OSI), contributing to a deeper understanding of atherosclerosis in cardiovascular disease.

Some studies have used fluid-structure interaction (FSI) models to account for arterial wall mechanics, including elasticity and deformation. The FSI study capture dynamic interactions between blood flow and compliant vessel walls, improving understanding of flow instabilities under pathological conditions. However, FSI modeling typically requires accurate patient-specific material properties and significantly more computational resources. In the current study, CFD-based simulations under rigid wall assumptions were adopted as a practical and validated method to isolate flow-related variables, such as velocity, pressure, and WSS, in geometrically idealized coronary bifurcation models. This approach is

consistent with a wide body of prior research and allows efficient comparison of multiple stenosis and bifurcation angle configurations. Finally, computational approaches, sophisticated imaging, and considerable research have shown the complex interconnections inside coronary artery bifurcations and the consequences on blood flow patterns, stenosis, and hemodynamic parameters. Even though a lot of area has been covered, more research has to be done to determine how exactly bifurcation angles affect the development and progression of coronary artery disorders. The aim of this research is to fill this gap in information by conducting a detailed computational investigation of how blood flow changes, especially near arterial bifurcations, cause and worsen coronary artery diseases.

This study uses 3D computer modeling to gain insight into how bifurcation angles and stenosis levels change the flow of blood in the coronary arteries. The purpose of this study is to employ numerical method to figure out how bifurcation angles affect the way blood flows in coronary arteries with different levels of stenosis. The study looks at flow velocity, pressure distribution, and wall shear stress to provide more information about how CAD develops and help us make more accurate diagnoses, assess risks, and plan treatments that are tailored to each person.

## 2. COMPUTATIONAL METHODOLOGY

It is evident that the majority of the coronary primary arteries exhibit bifurcation throughout their entire length. Stenosis commonly manifests in proximity to arterial bifurcations or places characterized by arterial bending.

### 2.1 Physical Model

The geometry of the artery was represented as a Y-shaped pipe. The 3D computer-aided design (CAD) program SOLIDWORKS was used to create the geometry model of the coronary artery. Figure 1 depicts the geometric outline of a coronary artery in good health. The main artery is 10 millimeters long, whereas the branch arteries are 20 and 25 millimeters long. Generally, in healthy volunteers, the left main and left anterior descending coronary arteries had an average length of 81.8 +/- 13.9 mm, whereas in patients, it was 76.2 +/- 16.5 mm [45]. Two arteries split from the main trunk at an angle of 47 degrees. Angles of 47° and 37° were selected because the bifurcation angle between the left anterior descending and the left main coronary artery (approximately 37.6°) is considered an inherently independent predictor, and there is a lot of variation in the anatomy of the coronary artery and its bifurcation angle (BA), which is different in people with and without distal CAD [47].

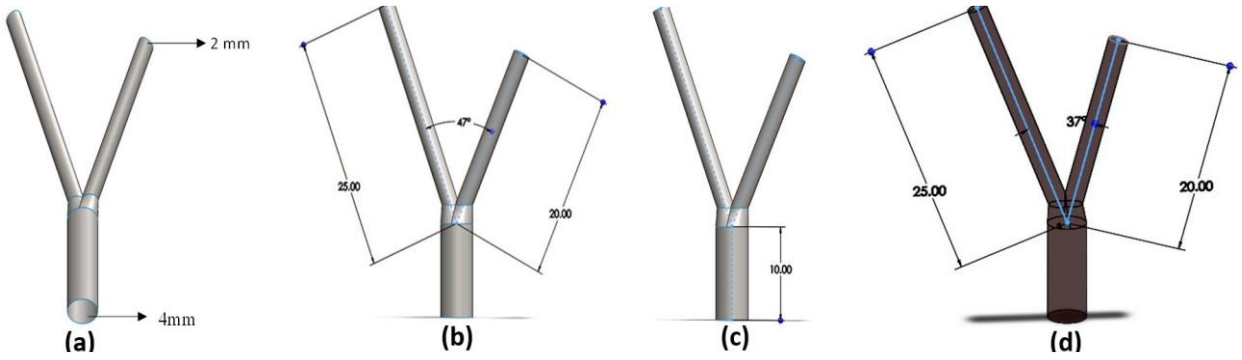


Figure 1. Healthy artery geometry with different angle

Both anatomical and clinical factors can affect the coronary artery bifurcation angle (BA). There is a 4 mm diameter at the inlet and a 2 mm diameter at the outlet. Each of these parts was built more easily using SolidWorks. Figure 2 indicates the conceptual geometric representation of diseased coronary artery. The stenotic area forms due to a constriction of the artery's core section. The stenosis adopts an eccentric form. Various degrees of stenosis, specifically 50%, 70%, and 85%, were assessed within the artery system. The quantification of stenosis percentage can be obtained through the application of the equation provided below [47]:

$$Percentageofstenosis = \left(1 - \frac{D_{stenosis}}{D_{normal}}\right) \times 100\backslash\% \quad (1)$$

where $D_{normal}$ = normal artery diameter and $D_{stenosis}$ = stenosis diameter.

### 2.2 Different Cases of Physiological Models

The current work presents two models involving the modification of the angle between branch arteries 47° and 37° while keeping the stenosis percentage the same. With a 50% stenosis, the artery's diameter is smaller because plaque has built up. In this case, the stenotic region of the main artery has a diameter of 4 mm, while the stenotic region of the branch artery has a diameter of 2 mm. Figure 2(a) and Figure 2(d) show how the artery looks when the stenosis is at a 50% level. This gives a clear picture of how the stenosis narrows the artery.

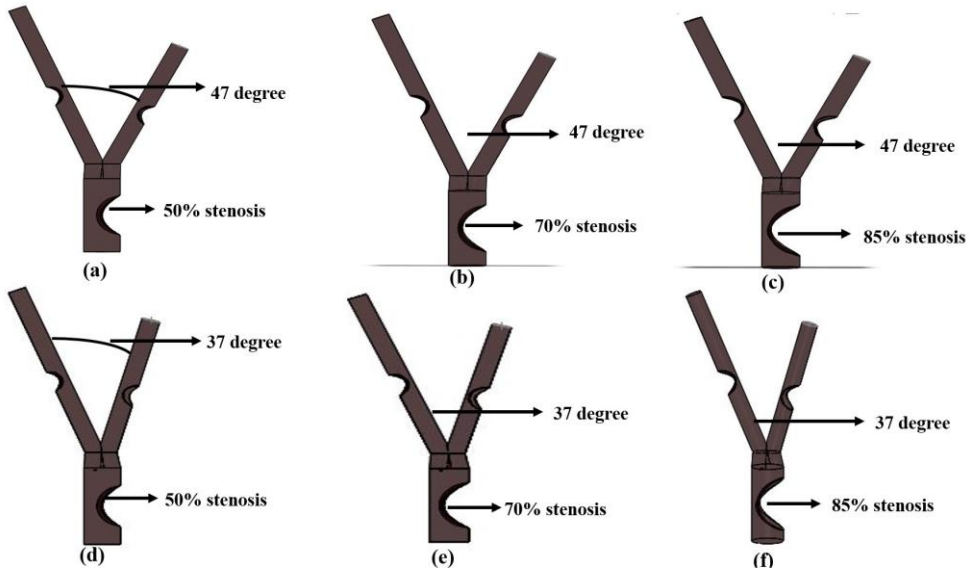


Figure 2. Geometry of the 47-degree angle between branch arteries: (a) 50% stenosis applied to both the main 4 mm artery and the two 2 mm branch arteries; (b) 70% stenosis in all three arteries; (c) 85% stenosis consistently applied to the main and both branch arteries. Geometry of the 37-degree angle between branch arteries: (d) 50% stenosis in the main and both branch arteries; (e) 70% stenosis in all arteries; (f) 85% stenosis applied equally across the main and 2 mm branches

When the stenosis gets worse to 70%, the effect of narrowing gets stronger. In particular, the effective lumen diameter is reduced to 1.2 mm in the main artery and 0.6 mm in the branch artery, corresponding to 70% stenosis. This higher amount of stenosis makes it harder for blood to flow, which changes how the blood moves through the artery. Figures 2 (b) and 2 (e) show how the cross-section of an artery looks when it has a 70% stenosis. This shows how the plaque buildup makes the artery narrower. Moving up the scale of stenosis severity, the study looks at what would happen if there was an 85% stenosis. In this case, the effective lumen diameter is further reduced to 0.6 mm in the main artery and 0.3 mm in the branch arteries, representing 85% stenosis. As shown in Figures 2 - (c) and (f), this advanced level of stenosis changes the shape of the artery in a big way, showing how much the serious narrowing affects blood flow. The flow division and distribution patterns inside the artery could be changed by changing the angle between branch arteries, potentially resulting in differences in wall shear stress and turbulence zones. In the present study, stenosis was applied both in the main artery and in the branch arteries to replicate a more clinically realistic scenario, where plaque buildup often occurs simultaneously at and near bifurcations. This approach allows for observing the combined hemodynamic effects of narrowing across all artery segments. While this work focuses on simultaneous plaque presence, future studies may explore comparative cases where stenosis occurs exclusively in the main artery or only in the branches. These isolated configurations were not included in the current analysis to maintain consistent conditions for evaluating bifurcation angle effects across varying stenosis severities.

## 3. NUMERICAL METHODOLOGIES

### 3.1 Governing Equation

We assume that blood flow inside the artery represents a non-Newtonian fluid and has a pulsatile flow, the equations that regulate blood flow are the same as those that govern the flow of any other type of fluid problem. The continuity equation and the momentum equation are considered the two sets of governing equations that are considered to be the most fundamental. The equations are summarized in the following way [48]:

$$\partial\rho/\partial t + \nabla \cdot (\rho v) = 0 \tag{2}$$

As a result of the fact that blood is an incompressible fluid, its rate of density change is constant; hence, the continuity equation that was presented earlier can be further simplified as follows:

$$\nabla \cdot v = 0 \tag{3}$$

$$\rho(v \cdot \nabla)v = -\nabla p + \mu\nabla^2 v \tag{4}$$

here, $\rho$, $V$, p and $\mu$ denotes density, blood velocity vector, pressure and viscosity. The viscosity coefficient varies as a function of shear rate and is hence not a constant. When the shear rate is increased, the blood becomes less viscous. The density of blood is considered as 1060 kg/m$^3$ [49]. Since blood is assumed to be a non-Newtonian fluid in this investigation, the Carreau viscosity non-Newtonian model is applied. The Carreau model is additionally recognized as the closest non-Newtonian model to support the clinical measurements [50]. The Carreau model can be expressed mathematically as follows:

$$\mu_{\text{eff}}\left(\dot{\gamma}\right)=\mu_{\text{inf}}+\left(\mu_0-\mu_{\text{inf}}\right)\left(1+\left(\lambda\dot{\gamma}\right)^2\right)^{\frac{n-1}{2}} \tag{5}$$

here, $\mu_{\text{eff}}$ is the effective viscosity, $\mu_{\text{inf}}$ is the infinite shear viscosity = 0.0035 kg·m$^{-1}$·s$^{-1}$, $\mu_0$ is the zero-shear viscosity = 0.056 kg·m$^{-1}$·s$^{-1}$, $\lambda$ is the time constant = 3.313 s, n is the power law index = 0.3568 and $\dot{\gamma}$ = shear rate.

### 3.2 Boundary Condition and Mesh Generation

The artery's outer wall is supposed to represent a rigid wall. The necessary boundary conditions are listed below:

Table 1. Boundary conditions

| Materials | Blood |
|---|---|
| Inlet | as proposed by Sinnott *et al.* [51] |
| Outlet | gauge pressure 13332 Pa |
| Reference values | area (as per geometry ), density (1060 kg/m$^3$, velocity (0.1 m/s) |
| Viscosity | carreau model |
| Arterial wall | no-slip and rigid |

In this study, blood was treated as a non-Newtonian fluid using the Carreau model. The sinusoidal rhythm is used to describe the periodic fluctuations in the inlet velocity during the systolic phase. Specifically, a pulsatile velocity profile was applied at the inlet, based on the waveform proposed by Sinnott *et al.* [51], with a maximum velocity of 0.5 m/s and a minimum velocity of 0.1 m/s over a period of 1 second. This profile was generated using a user-defined function (UDF) in ANSYS Fluent to show how blood flow at both high and low speeds affects things. The inlet part was circular and had a 4 mm diameter, which was the main coronary artery.

A gauge pressure of 13,332 Pa (100 mmHg) was applied at the outlet to simulate typical back-pressure conditions. The arterial wall was modelled as being rigid and having a no-slip boundary condition, which indicated that the blood flow velocity at the wall surface was thought to be zero. These assumptions make the model easier to work with and keep the focus on how bifurcation angle and stenosis severity affect things. The graph of inlet velocity profile is given below [52]:

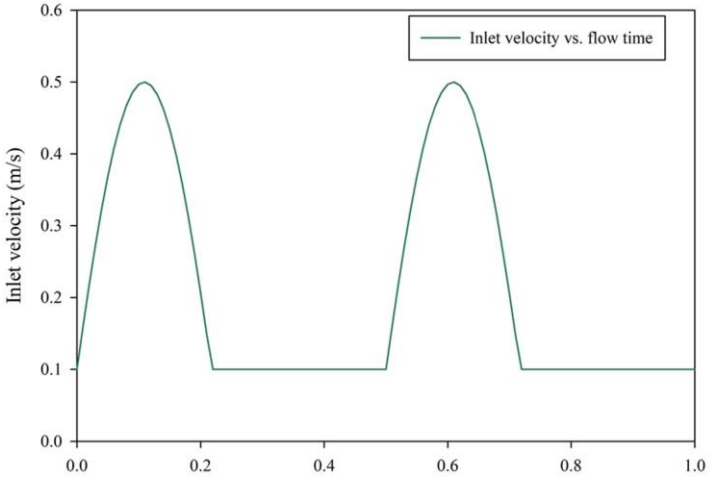


Figure 3. Pulsatile (cardiac cycle) flow velocity profile

### 3.3 Suitable Grid Generation

In the field of numerical simulations, especially when dealing with complex phenomena like hemodynamics, creating a good grid or mesh in 3D computing is a basic and important step. This finite element (FE) method includes constructing a grid-like structure to represent the domain's geometry, which often consists of an enormous number of tiny elements or grid cells. The success of the simulation depends heavily on the quality and accuracy of this mesh. Both normal and stenotic arterial meshes are shown in Figures 4 (a) and 4(c) respectively. These images shed light on how stenotic lesions, which cause narrowing and irregularities in the arteries, are accounted for during the meshing process. The geometry under consideration is meshed using tetrahedral elements.

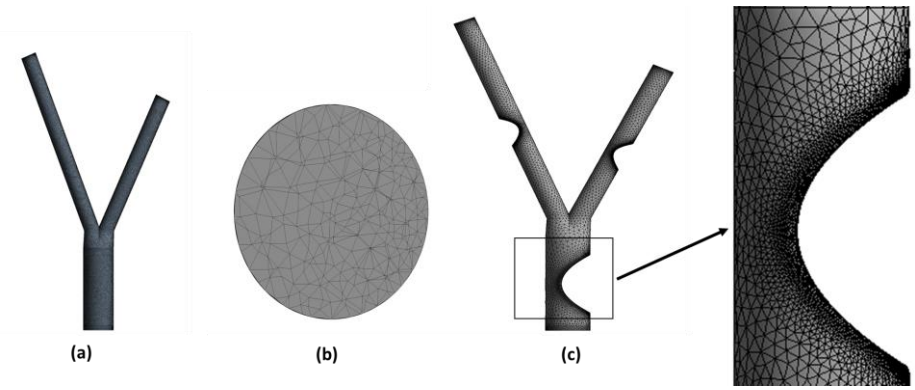


Figure 4. Mesh generation of (a) healthy artery, (b) inlet section and (c) diseased artery

### 3.4 Grid Independence Test

The bifurcation model, exposed to dynamic simulations at a 47-degree angle, conducted a sensitivity analysis to discover the appropriate element size for computations. Table 2 presents details on the seven resulting grids used to test the accuracy of the findings. The model's materials and structure remained identical throughout all of these computer simulations. Instead, the shear stress on the wall was measured, recorded, and compared to previous findings when the number of meshes was changed. This process proceeded until the difference between the current simulation and the previous one was less than 0.002. The study found that the best mesh conditionality for the 47-degree model is 330,582, and that all simulations should use an element size of about 1.95 mm.

Table 2. Grid independence test

| Size of elements mm | Number of elements | Wall Shear Stress (WSS) | $\frac{\lvert WSS_{i+1} - WSS_i \rvert}{WSS_{i+1}}$ |
|---|---|---|---|
| 3.50 | 55981 | 4.812 | - |
| 3.20 | 65198 | 4.956 | 0.029 |
| 2.80 | 78403 | 4.929 | 0.005 |
| 2.40 | 87905 | 5.135 | 0.040 |
| 2.20 | 104470 | 5.394 | 0.048 |
| 2.02 | 176209 | 5.899 | 0.085 |
| 1.95 | 330582 | 5.891 | 0.001 |
| 1.92 | 362432 | 5.915 | 0.004 |
| 1.75 | 381352 | 5.926 | 0.002 |

### 3.5 Numerical Validation for the Simulation Result

A validation study was carried out to ensure the computational model was accurate by comparing the results of the current simulation with data that Khademi *et al.* [23] had already published. The validation was carried out under steady-state flow conditions to match the reference study's parameters, allowing a direct comparison of key hemodynamic outputs. We employed a pulsatile inlet waveform (0.5–0.1 m/s) that was set up using a user-defined function, as explained in Section 3.2. The finite element (FE) method with tetrahedral elements was employed to mesh the geometry, which included both normal and stenotic arterial segments. A structured analysis was performed to look at the quality and sensitivity of the mesh. For example, for the bifurcation model with a 47-degree angle, we ran a mesh independence test by making seven different mesh densities, which are shown in Table 2. As the mesh became better, we kept an eye on the simulation results, especially the wall shear stress. We kept doing the process until the difference between the outcomes was less than 0.002, which meant that the measurements were converging. The mesh resolution and boundary conditions were matched as closely as possible to those used in the original study, including inlet velocity profiles, outlet pressure conditions, and wall properties As shown in Figure 5, the results from the present simulation closely follow the trend of Khademi *et al.* [23] with minimal deviation in both maximum velocity and cross-sectional area across all tested angles. The results exhibit strong agreement, confirming the accuracy and validity of the current CFD model in predicting hemodynamic behavior within coronary bifurcation geometries.

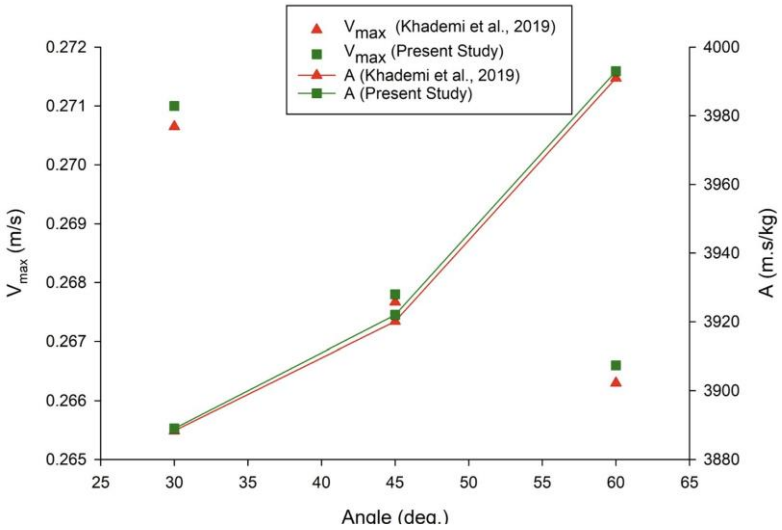


Figure 5. Relationship between present and existing study [23]

### 3.6 Computational Resources

The 3D artery geometries were created using SolidWorks software (version not specified) and all computational fluid dynamics simulations were performed in ANSYS Fluent (version 2022 R2). Simulations were run on a workstation equipped with an Intel Xeon processor (2.6 GHz), 64 GB RAM, and Windows 10. The solver operated in double-precision mode, and each simulation required several hours of computation time to achieve convergence.

## 4. RESULTS AND DISCUSSION

This research aims to examine how idealized models of bifurcated healthy and plagued arteries, with 37 degree and 47-degree bifurcation angles, affect the properties of coronary blood flow. One category of models represented a coronary artery in good condition, whereas the other set simulated coronary artery disease with three different stenosis and angle variations. The primary objective of this investigation is to establish a comprehensive framework for reconstructing a simplified representation of the coronary artery, analyze its geometric features, and elucidate the associated hemodynamic properties, including blood flow velocity, pressure differentials, and wall shear stress. To determine the hemodynamic components, the simulations were run for a flow time of 1 second to look at the effects. In order to evaluate the effects of flow velocity, WSS, and pressure differential high magnitudes, respectively, one timesteps has been recorded t = 0.63s, where the velocity is at peak. In the study, we showcased the hemodynamic metrics at t = 0.63 s for all scenarios. To provide a comprehensive understanding of the current artery investigation, Figures 6–12 present the distributions of WSS, velocity, and pressure at different 2-D planes of the fluid domain, under all conditions at a variable time of t = 0.63 s.

### 4.1 Effect of Velocity Distribution

Figures 6 show the velocity distribution contours of plane-1 at times t = 0.63 s where plane-1 is the mid-plane of the whole domain. As seen in the figure, treating blood as a non-Newtonian fluid has a major impact on velocity distributions and the associated disturbances. The entrance velocity distribution at the larger-diameter inlet is the 0.54 m/s at t = 0.63s.

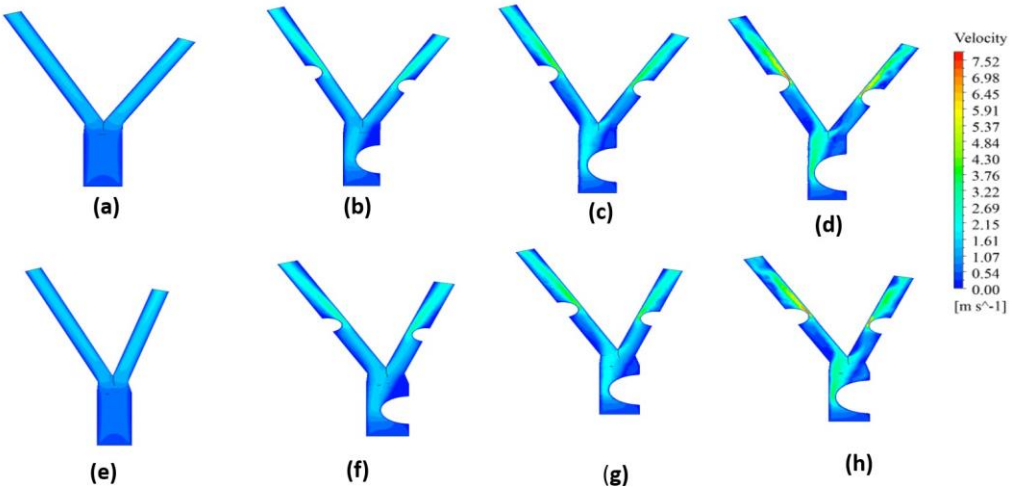


Figure 6. Flow velocity contour at t = 0.63 s - 47-degree angle of (a) healthy artery (b) 50% stenosis (c) 70% stenosis (d) 85% stenosis, 37-degree angle of - (e) healthy artery (f) 50% stenosis (g) 70% stenosis (h) 85% stenosis

At t = 0.63 s, the velocity contour for blood flow for healthy artery has increased to approximately 1.51 m/s [Fig. 6 (a) and (e)]. Based on the contours observed, it appears that there is minimal disturbance and blood mixing happening, as there are no stenoses present that could obstruct the flow of blood. Additionally, the bifurcated zone indicates a smooth transition between the two branches, which is a positive sign. Subsequently, at t = 0.63 s in the 50% stenosis area, it reaches approximately 2.15 m/s [Figure 6 (b) and (f)] and in Figure 6 (c) and (g), at 70% stenosis area it reaches approximately 2.69 m/s.

Notably, in instances of jetting blood flow, high velocity values are recorded due to small gaps in the stenosis, and visible flow recirculation is observed in Figure 6 - (d) and (h). The researcher observed that the velocity increase at the stenosis area is approximately 3.22 m/s in the main artery, while in branch arteries stenosis, it exceeds approximately 3.52 m/s. The velocity contour plot of a cross-section in the mid-section (halfway along its vertical height) of the model is displayed in Figure 7. The comparison between CFD results generated using various time steps and the experimental velocity measurements plotted horizontally is shown here.

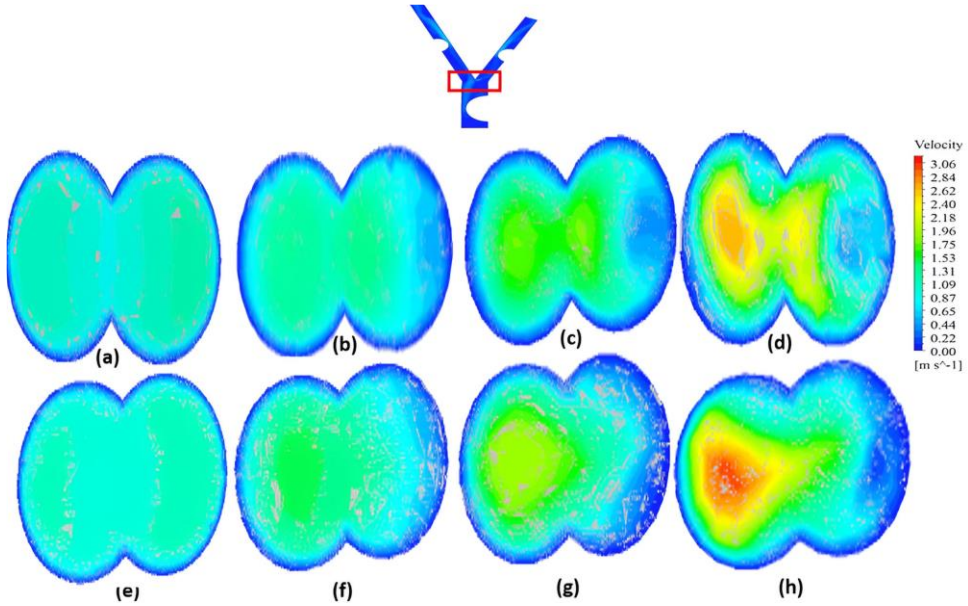


Figure 7. Flow velocity contour at t = 0.63 s along the length of the artery(a) 47-degree angle of healthy artery, 47-degree angle of - (b) 50% stenosis (c) 70% stenosis (d) 85% stenosis, (e) 37-degree angle of healthy artery, 37- degree angle of - (f) 50% stenosis (g) 70% stenosis (h) 85% stenosis

### 4.2 Effect of Pressure Distribution

Results from 3D idealized model of pressure distribution in different physiological situations were shown in this part. The time evolution of the pressure drops at the time step 0.63 s is shown in Figure 8. Analyzing Figure 8 reveals that there is a discernible increase in pressure. At 0.63 s, the pressure within the 50% and 70% lesion areas ranges from 165 to 212 mmHg approximately, as depicted in Figure 8 (c) and (g). However, in proximity to the 85% stenosis areas, the pressure escalates significantly, reaching levels of 260 to 330 mmHg, as illustrated in Figure 8 (d) and (h). Notably, the elevated pressure is more pronounced in the regions of stenosis in the branch arteries compared to the primary artery.

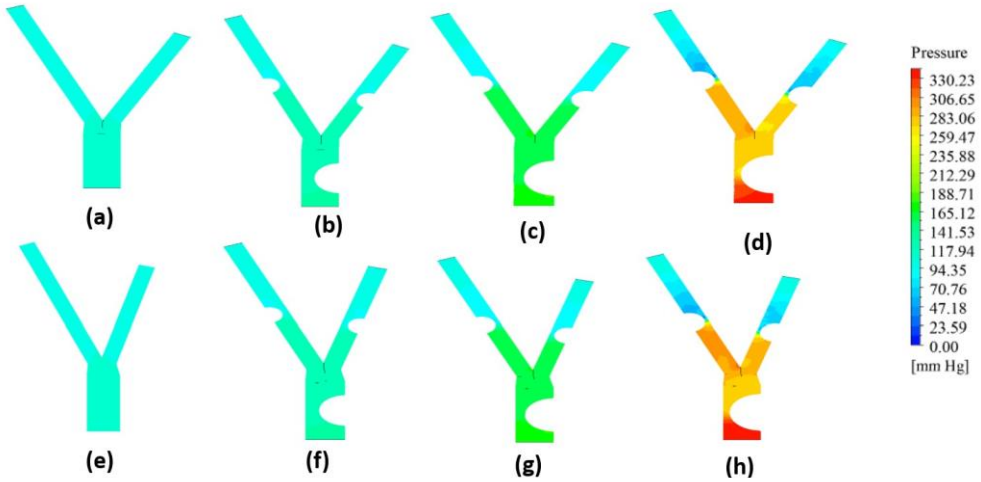


Figure 8. Pressure field of the 3D idealized model at t = 0 .63 s (a) 47-degree angle of healthy artery, 47- degree angle of - (b) 50% stenosis (c) 70% stenosis (d) 85% stenosis, (e) 37-degree angle of healthy artery, 37- degree angle of - (f) 50% stenosis (g) 70% stenosis (h) 85% stenosis

The pressure slice figure clearly illustrates this. Examining the pressure slices depicted in Figures 9, it becomes evident that fluctuations in pressure severity, influenced by the conditions of stenosis and the angles of the branch arteries. The pressure slice figure is given below:

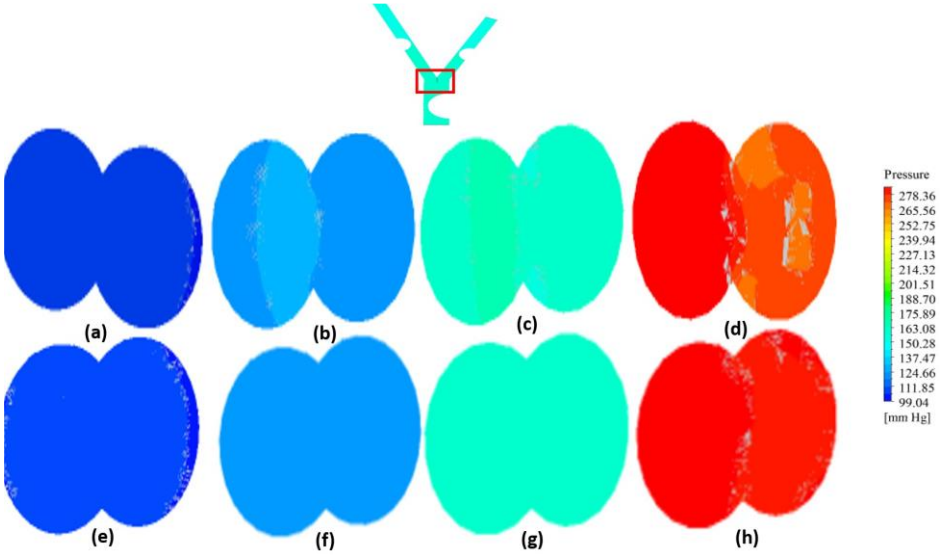


Figure 9. Pressure field slice of the idealized 3D model at t = 0.63 s (a) 47-degree angle of healthy artery, 47- degree angle of - (b) 50% stenosis (c) 70% stenosis (d) 85% stenosis, (e) 37-degree angle of healthy artery, 37- degree angle of - (f) 50% stenosis (g) 70% stenosis (h) 85% stenosis

Moving to t = 0.63 s, the pressure remains normal in the healthy artery (Figures 9 (a) and (e)). Subsequently, as time progresses, the pressure gradually increases due to angle and stenosis severity variations. In the case of 50% stenosis, the pressure reaches almost 130 mmHg (Fig. 9 (b) and (f)), while in 70% stenosis, it rises to approximately 170 mmHg (Fig. 9 (c) and (g)). In the 85% stenosis with a 47-degree angle, the pressure peaks at almost 270 mmHg (Fig. 9 (d)), exceeding 330 mmHg for the 37-degree angle (Fig. 9 (h)). Notably, even slight differences in angle result in corresponding changes in pressure (Figure 9 (h)).

### 4.3 Effect of WSS Distribution

The behavior of the arterial wall is greatly affected by wall shear stress. Stenosis is well known to be correlated with shear stress operating on the walls of arteries. The shear stress on a wall is proportional to the geometrical differences and the velocity fluctuations near the wall. When the shape of an artery changes, the blood flow changes as well. Shear stress rises at points when flow enters a narrow passage, which might be an obstruction or a bifurcation. Figures 10 shows the three-dimensional wall shear stress contours at the chosen times of 0.63 s, respectively.

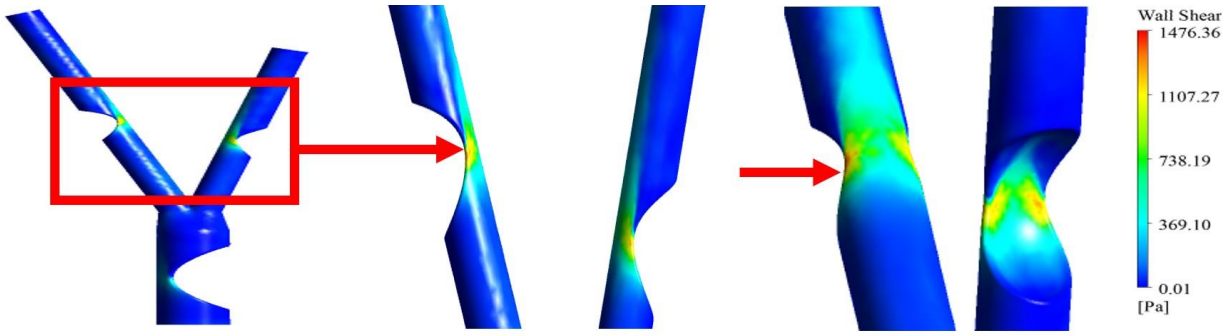


Figure 10. Wall shear stress of the 3D idealized model at t = 0 .63 [s] at 85% stenosis

At t = 0.63 seconds, the 85% stenosis region undergoes a significant change, with an approximate peak wall shear stress of 78 Pa near the stenosis area of the branch arteries [Figure 10].

### 4.4 Effect of Artery Wall Pressure Distribution

Figures 11 depict the pressure exerted on the artery wall due to fluid exchanges at certain time intervals. The pressure of the vessel wall aligns with the values specified in the legend. Initially at t = 0.63 seconds the pressure remains at 100 mmHg for healthy and 50% stenosis arteries [Figure 11 (a), (b), (e), (f)], it increases to 180 mmHg in the 70% stenosis region [Figure 11 (c) and (g)]. In the vicinity of branch arteries' stenosis regions, the pressure rises to 270 mmHg, and near the main arteries' stenosis regions, it exceeds 330 mmHg [Figure 11 (d) and (h)].

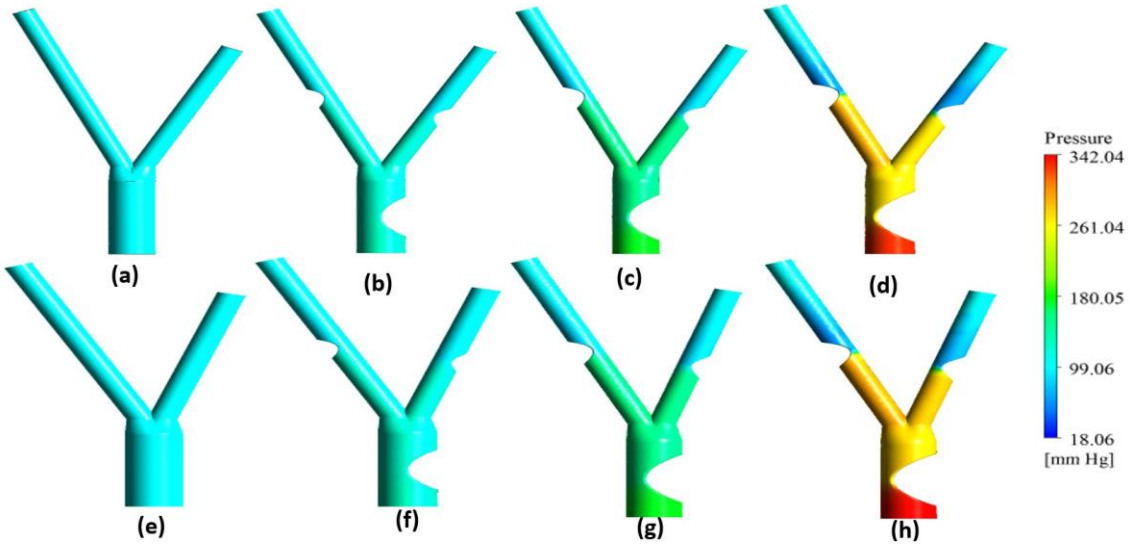


Figure 11. Wall pressure of the 3D idealized model at t = 0 .63 s (a) 47-degree angle of healthy artery, 47- degree angle of - (b) 50% stenosis (c) 70% stenosis (d) 85% stenosis, (e) 37-degree angle of healthy artery, 37- degree angle of - (f) 50% stenosis (g) 70% stenosis (h) 85% stenosis

### 4.5 Streamline Visualization

Based on Figure 12, it can be observed that the behavior of the flow changes as the degree of stenosis increases and the pathway becomes narrower. When there is no stenosis, the flow pattern is calm and produces less turbulence. However, as the stenosis increases, the flow pattern becomes more turbulent. In particular, Figure 12(b) and (f) depict the streamline at the bifurcation zone for 47 and 37 degrees with 50% stenosis. Although the area reduction is the same, there is a slight variation due to the angle, and as a result, the 47-degree 50% stenosis experiences more turbulence. This trend is also visible for the other cases, such as 70% and 85% stenosis for 47-degree, which produces higher vortices compared to 37 degrees. This indicates that there is a higher wall pressure and WSS at a higher bifurcation angle. It is noted that streamlines are presented only in the bifurcation region to highlight local flow patterns and recirculation. For the full flow field from inlet to outlet, please refer to the velocity contours shown in Figures 6 and 7.

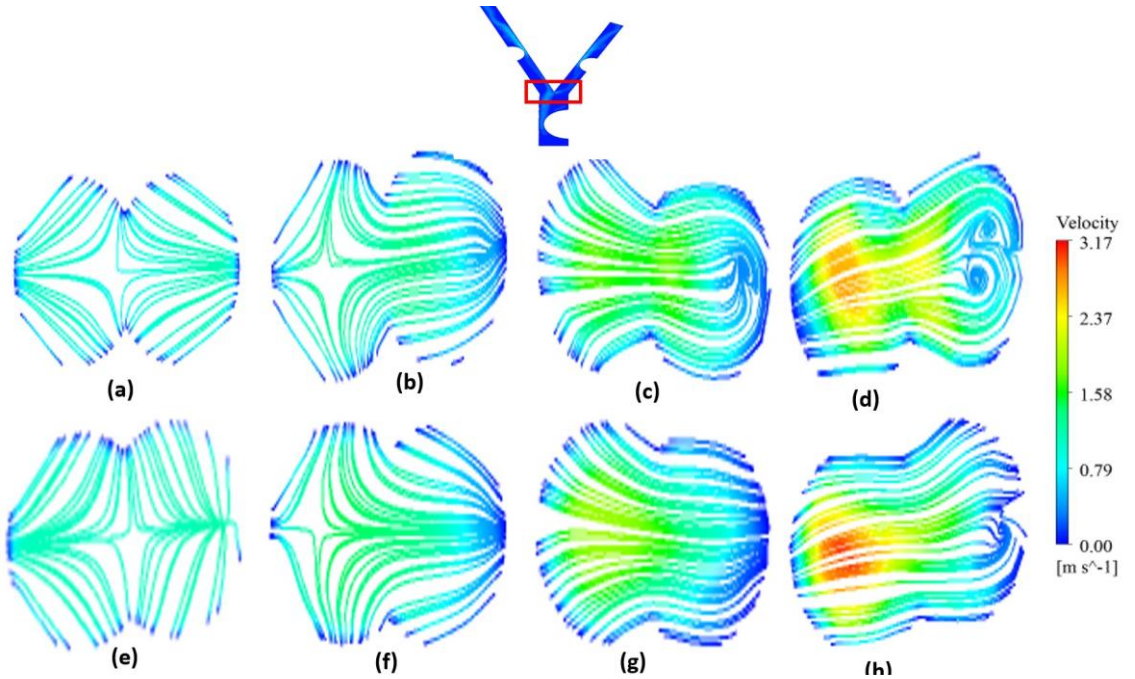


Figure 12. Streamline of the 3D idealized model at t = 0 .63 s (a) 47-degree angle of healthy artery, 47- degree angle of - (b) 50% stenosis (c) 70% stenosis (d) 85% stenosis, (e) 37-degree angle of healthy artery, 37- degree angle of - (f) 50% stenosis (g) 70% stenosis (h) 85% stenosis

### 4.6 Effect of Flow time in Hemodynamic Parameters

This section presents a graphical comparison of pressure, wall shear stress (WSS), and artery wall pressure observed at bifurcation angles of 47° and 37°, highlighting the hemodynamic variations associated with different stenosis severities.

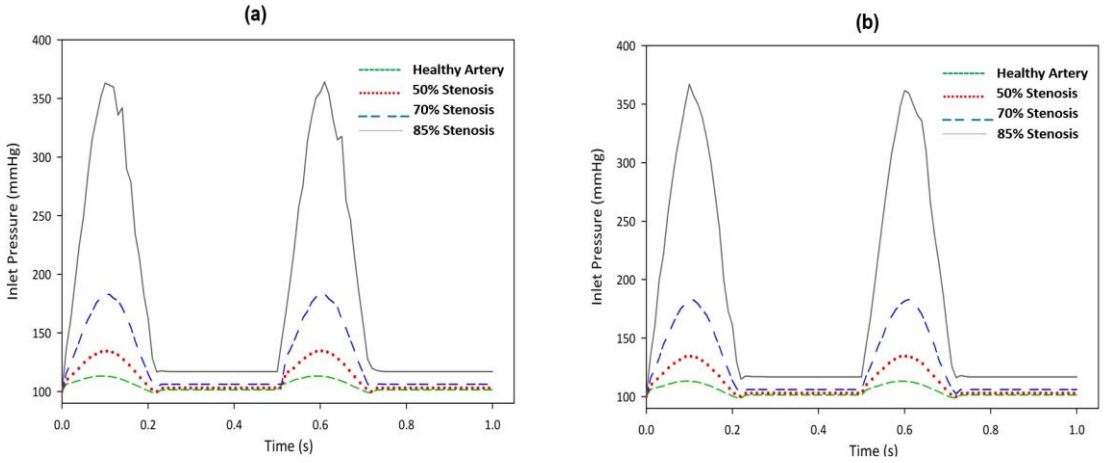


Figure 13. Graphical view of – (a) 47-degrees inlet pressure (b) 37-degrees inlet pressure

In Figure 13, it is evident that inlet pressure increases with stenosis severity. Compared to the healthy artery, the inlet pressure rises by approximately 23% in 50% stenosis, 54% in 70% stenosis, and 177% in 85% stenosis.

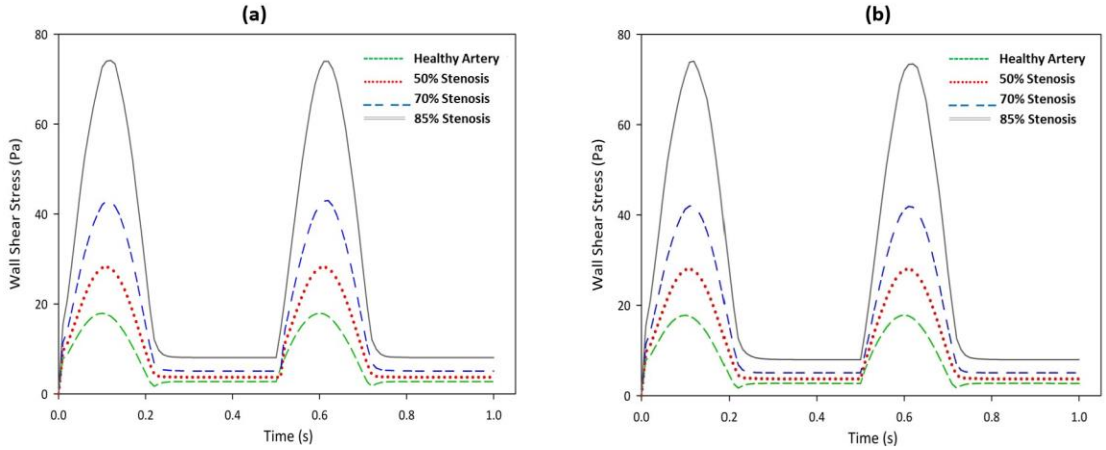


Figure 14. Graphical view of – (a) 47 degrees wall shear stress (b) 37 degrees wall shear stress

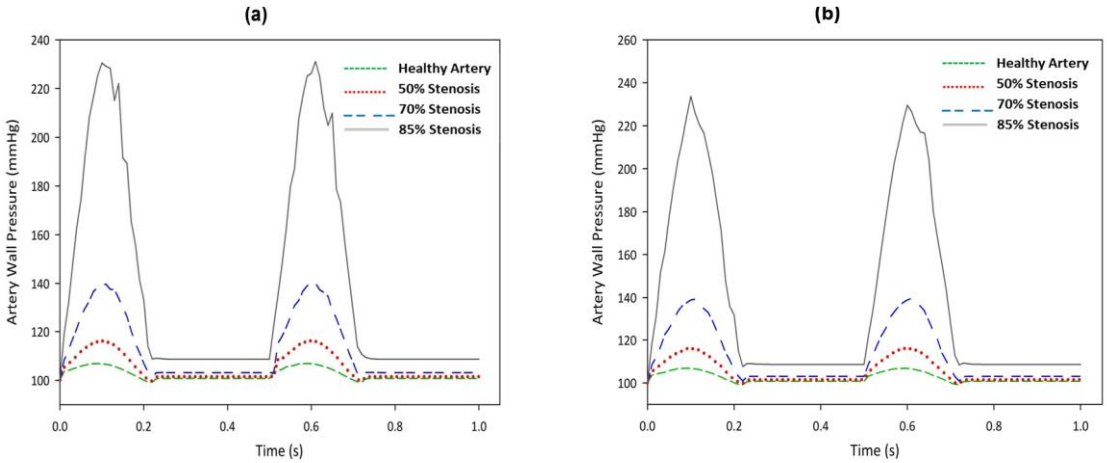


Figure 15. Graphical view of – (a) 47 degrees artery wall pressure (b) 37 degrees artery wall pressure

Figures 14 and 15 show similar trends for WSS and artery wall pressure. WSS increases from 17 Pa in the healthy artery to 59% higher in 50% stenosis, 135% higher in 70% stenosis, and 324% higher in 85% stenosis. Artery wall pressure also rises significantly, with increases of approximately 17%, 39% and 100% compared to the healthy condition. These percentage differences clearly demonstrate the substantial hemodynamic impact of increasing stenosis severity. Here is the table showing the percentage increase in each parameter (wall shear stress, inlet pressure, artery wall pressure) for 50%, 70%, and 85% stenosis compared to a healthy artery.

Table 3. Percentage increase in hemodynamic parameters for different stenosis severities compared to a healthy artery

| | 50% Stenosis | 70% Stenosis | 85% Stenosis |
|---|---|---|---|
| Inlet Pressure (mmHg) | 23.07 | 53.85 | 176.92 |
| Wall Shear Stress (Pa) | 58.82 | 135.30 | 323.53 |
| Artery Wall Pressure (mmHg) | 17.39 | 39.13 | 100.00 |

### 4.7 Discussion of Model Limitations and Future Work

This study simulated coronary blood flow over a single cardiac cycle using a sinusoidal inlet velocity waveform and assumed rigid arterial walls. While this approach captures key pulsatile effects, it does not consider multiple consecutive cardiac cycles or the dynamic motion of the heart, which can further influence flow patterns and wall shear stress. Kim *et al.* [53] used FSI to capture dynamic blood flow-compliant vessel wall interactions to better understand flow instabilities under pathological situations. FSI modeling demands patient-specific material features and greater computer resources. Recent research [54] highlights that multi-cycle simulations and fluid–structure interactions provide a more comprehensive representation of coronary hemodynamic. Additionally, the use of idealized geometries may limit direct clinical translation. Future work could incorporate patient-specific geometries, multi-cycle simulations, and deformable wall models to enhance physiological accuracy and clinical relevance.

## 5. CONCLUSIONS

This study utilized CFD simulations to examine how stenosis severity and bifurcation angle influence coronary artery blood flow, using idealized 3D models and a non-Newtonian blood flow assumption. The analysis revealed that severe stenosis (up to 85%) significantly increases velocity, wall shear stress, and pressure, particularly near arterial bifurcations with larger angles. Peak values reached approximately 3.52 m/s for velocity, 78 Pa for WSS, and 230 mmHg for pressure, identifying critical regions susceptible to disease progression. These findings enhance understanding of the relationship between arterial geometry and hemodynamic abnormalities, providing valuable insights that may improve early diagnosis and inform targeted treatments for coronary artery disease. However, the study is limited to idealized artery models and inlet is pulsatile, not steady; future work could extend to patient-specific geometries and pulsatile flow to better capture physiological variability.

## ACKNOWLEDGEMENTS

The authors express their gratitude to the Faculty of Engineering at Ahsanullah University of Science and Technology (AUST) and the International Islamic University Malaysia (IIUM) for their technical support. Special thanks are due to the computational laboratories for providing access to the high-performance computing resources required for the CFD simulations.

## CONFLICT OF INTEREST

The authors declare no conflicts of interest.

## AUTHORS' CONTRIBUTION

S.H. Maowa (Data Collection, Software Management, Designed the Analysis and Drafted the Manuscript)

M.M. Billah (Study Conception, Supervision, Design, Final Manuscript Preparation)

K.E. Hoque (Data Analysis, Supervision, Final Draft of the Manuscript)

N.F. Ifraj (The Idea of the Work, Primary Draft Writing)

M.S. Hossain (Visualisation; Supervision)

S.M.A. Hoq (Study Conception, Design Final Manuscript Preparation)

## AVAILABILITY OF DATA AND MATERIALS

The datasets generated during and/or analysed during the current study are available from the corresponding author on reasonable request.

## ETHICS STATEMENT

This study did not involve human participants or animals. Ethical approval was therefore not required.

## REFERENCES

[1] K. E. Hoque, M. Ferdows, S. Sawall, E. E. Tzirtzilakis, M. A. Xenos, "Hemodynamic characteristics expose the atherosclerotic severity in coronary main arteries: One-dimensional and three-dimensional approaches," *Physics of Fluids*, vol. 33, no. 12, pp. 1–13, 2021.

[2] S. Malek, A. Eskandari, M. Sharbatdar, "Machine learning-based prediction of hemodynamic parameters in left coronary artery bifurcation: A CFD approach," *Heliyon*, vol. 11, no. 2, p. e41973, 2025.

[3] J. Yang, Y. Zhang, J. Xue, S Liu, Y Yao, H Zhong, et al., "Hemodynamic effects of stenosis with varying severity in different segments of the carotid artery using computational fluid dynamics," *Scientific Reports*, vol. 15, p. 4896, 2025.

[4] T. Chaichana, Z. Sun, J. Jewkes, "Hemodynamic impacts of various types of stenosis in the left coronary artery bifurcation: A patient-specific analysis," *Physica Medica*, vol. 29, no. 5, pp. 447–452, 2013.

[5] M. Farajtabar, M. M. Larimi, M. Biglarian, D. Sabour, M. Miansari, "Machine learning identification framework of hemodynamics of blood flow in patient-specific coronary arteries with abnormality," *Journal of Cardiovascular Translational Research*, vol. 16, no. 3, pp. 722–737, 2022.

[6] N. Alzhanov, E. Y. K. Ng, Y. Zhao, "Hybrid CFD PINN FSI simulation in coronary artery trees," *Fluids*, vol. 9, no. 12, p. 280, 2024.

[7] R. Gharleghi, M. Zhang, C. Shen, M. Webster, C. Ellis, S. Beier, "Assessing left main bifurcation anatomy and haemodynamics as a surrogate for disease risk in suspected coronary artery disease without stenosis," *Scientific Reports*, vol. 15, p. 254, 2025.

[8] S. Kamangar, I. A. Badruddin, A. E. Anqi, C. Ahamed Saleel, V. Tirth, T. M. Yunus Khan, et al., "Influence of bifurcation angle in left coronary artery with stenosis: A CFD analysis," *Bio-Medical Materials and Engineering*, vol. 31, no. 6, pp. 339–349, 2020.

[9] A. Candreva, G. D. Nisco, M. L. Rizzini, F. D'Ascenzo, G. M. De Ferrari, D. Gallo. et al., "Current and future applications of computational fluid dynamics in coronary artery disease," *Reviews in Cardiovascular Medicine*, vol. 23, no. 11, p. 377, 2022.

[10] M. Nikpour, A. Mohebbi, "Predicting coronary artery occlusion risk from noninvasive images by combining CFD-FSI, cGAN and CNN," *Scientific Reports*, vol. 14, p. 22693, 2024.

[11] B. Morgan, A. R. Murali, and G. Preston, Y. A. Sima, L. A. Marcelo Chamorro, C. Bourantas, et al., "A physics-based machine learning technique rapidly reconstructs the wall-shear stress and pressure fields in coronary arteries," *Frontiers in Cardiovascular Medicine*, vol. 10, p. 1221541, 2023.

[12] H. G. Choi, D. H. Vo, J. Y. Yoo, S. T. Ha, K. Y. Lee, "The influence of reverse flow within side branches on plaque formation relative to coronary bifurcation angles," *Scientific Reports*, vol. 15, p. 11977, 2025.

[13] A. Müftüoğulları, M. Süner, B. Sarper, "The effect of bifurcation angulation on flow characteristics and hemodynamic indicators in an idealized left coronary artery," *International Journal of Thermofluids*, vol. 21, p. 100554, 2024.

[14] S. Zhao, W. Wu, and S. Samant, B. Khan, G. S. Kassab, Y. Watanabe, et al., "Patient-specific computational simulation of coronary artery bifurcation stenting," *Scientific Reports*, vol. 11, p. 16486, 2021.

[15] G. Li, H. Wang, and M. Zhang, S. Tupin, A. Qiao, Y. Liu, et al., "Prediction of 3D cardiovascular hemodynamics before and after coronary artery bypass surgery via deep learning," *Communications Biology*, vol. 4, p. 99, 2021.

[16] P. E. P. Carvalho, J. L. Cavalcante, and J. Lesser, V. Cheng, D. Strepkos, M. Alexandrou. et al., "Coronary CTA-guided bifurcation PCI," *JACC: Case Reports*, vol. 30, no. 2, p. 102814, 2025.

[17] M. F. Rabbi, F. S. Laboni, M. T. Arafat, "Computational analysis of the coronary artery hemodynamics with different anatomical variations," *Informatics in Medicine Unlocked*, vol. 19, pp. 1–10, 2020.

[18] H. Bouteloup, J. G. O. Marinho, S. Chatpun, D. M. Espino, "Computational analysis to predict the effect of pre-bifurcation stenosis on the hemodynamics of the internal and external carotid arteries," *Journal of Mechanical Engineering and Sciences*, vol. 14, no. 3, pp. 7029–7039, 2020.

[19] M. A. H. Mohd Adib, L. S. Hong, M. S. Abdullah, R. Hassan, S. Wada, "A perspective review: Technical study of combining phase contrast magnetic resonance imaging and computational fluid dynamics for blood flow on carotid bifurcation artery," *Journal of Mechanical Engineering and Sciences*, vol. 14, no. 4, pp. 7609–7621, 2020.

[20] S. Nayak, H. S. N. Kumar, S. M. A. Khader, R. Pai, "Effect of dome size on flow dynamics in saccular aneurysms—A numerical study," *Journal of Mechanical Engineering and Sciences*, vol. 14, no. 3, pp. 7181–7190, 2020.

[21] A. Belaghit, B. Aour, M. Larabi, A. A. Tadjeddine, S. Mebarki, "Numerical study of hemodynamics after stent implantation during the cardiac cycle," *Journal of Mechanical Engineering and Sciences*, vol. 15, no. 2, pp. 8016–8028, 2021.

[22] S. Ramli, R. Kamil, S. A. Ahmad, N. Mohtaruddin, R. Mahmud, "Wavelet transform based features of skin blood flow response signal for pressure ulcer evaluation," *Journal of Mechanical Engineering and Sciences*, vol. 14, no. 3, pp. 7309–7318, 2020.

[23] M. Khademi, A. Nikoo, S. Rahimnezhad, B. Jooghi, "CFD analysis of the blood flow in left coronary bifurcation with variable angulation," *International Journal of Biomedical and Biological Engineering*, vol. 13, no. 3, pp. 92–99, 2019.

[24] S. E. Razavi, V. Farhangmehr, Z. Babaie, "Numerical investigation of hemodynamic performance of a stent in the main branch of a coronary artery bifurcation," *BioImpacts*, vol. 9, no. 2, pp. 97–103, 2019.

[25] D. G. Owen, D. C. de Oliveira, E. K. Neale, D. E. T. Shepherd, D. M. Espino, "Numerical modelling of blood rheology and platelet activation through a stenosed left coronary artery bifurcation," *PLoS ONE*, vol. 16, no. 11, pp. 1–26, 2021.

[26] K. E. Hoque, M. Ferdows, S. Sawall, E. E. Tzirtzilakis, "The effect of hemodynamic parameters in patient-based coronary artery models with serial stenoses: Normal and hypertension cases," *Computer Methods in Biomechanics and Biomedical Engineering*, vol. 23, no. 9, pp. 467–475, 2020.

[27] G. Lorenzini, E. Casalena, "CFD analysis of pulsatile blood flow in an atherosclerotic human artery with eccentric plaques," *Journal of Biomechanics*, vol. 41, no. 9, pp. 1862–1870, 2008.

[28] T. Tsugu, K. Tanaka, Y. Nagatomo, D. Belsack, J. F. Argacha, B. Cosyns, et al., "Impact of ramus coronary artery on computed tomography derived fractional flow reserve (FFRCT) in no apparent coronary artery disease," *Echocardiography*, vol. 40, no. 2, pp. 103–112, 2023.

[29] G. N. Nagaharish, A. Buradi, P. V. Deshpande, N. B. Hallad, A. Madhusudhan, J. Bora, "Blood flow analysis through bifurcated and stenosed coronary artery," *Fluid Mechanics and Fluid Power*, vol. 2, pp. 7–12, 2023.

[30] S. Kamangar, N. J. Salman Ahmed, I. A. Badruddin, N. Al-Rawahi, A. Husain, K. Govindaraju, et al., "Effect of stenosis on hemodynamics in left coronary artery based on patient-specific CT scan," *Biomedical Materials and Engineering*, vol. 30, no. 4, pp. 463–473, 2019.

[31] S. Givehchi, M. J. Safari, S. K. Tan, M. N. B. M. Shah, F. M. Sani, R. R. Azman, et al., "Measurement of coronary bifurcation angle with coronary CT angiography: A phantom study," *Physica Medica*, vol. 45, pp. 198–204, 2018.

[32] K. Temov, Z. Sun, "Coronary computed tomography angiography investigation of the association between left main coronary artery bifurcation angle and risk factors of coronary artery disease," *International Journal of Cardiovascular Imaging*, vol. 32, pp. 129–137, 2016.

[33] S. Ali, C. Y. Ho, C. C. Yang, S. H. Chou, Z. Y. Chen, W. C. Huang, et al., "Computational fluid dynamics modeling of coronary artery blood flow using OpenFOAM: Validation with the Food and Drug Administration benchmark nozzle model," *Journal of X-Ray Science and Technology*, vol. 32, no. 4, pp. 1121–1136, 2024.

[34] Y. T. Katakia, S. Kanduri, R. Bhattacharyya, S. Ramanathan, I. Nigam, B. V. R. Kuncharam, et al., "Angular difference in human coronary artery governs endothelial cell structure and function," *Communications Biology*, vol. 5, p. 1044, 2022.

[35] A. Dhungana, A. Buradi, P. Dahal, B. J. Bora, "Impact of bifurcation and bifurcation angle on the hemodynamics of coronary arteries," *Fluid Mechanics and Fluid Power*, vol. 3, pp. 31–36, 2023.

[36] S. K. Shanmugavelayudam, D. A. Rubenstein, W. Yin, "Effect of geometrical assumptions on numerical modelling of coronary blood flow under normal and disease conditions," *Journal of Biomechanical Engineering*, vol. 132, no. 6, p. 061004, 2010.

[37] M. Jahangiri, M. Saghafian, M. R. Sadeghi, "Numerical simulation of non-Newtonian models effect on hemodynamic factors of pulsatile blood flow in elastic stenosed artery," *Journal of Mechanical Science and Technology*, vol. 31, no. 2, pp. 1003–1013, 2017.

[38] M. Lashgari, R. P. Choudhury, A. Banerjee, "Patient-specific in silico three-dimensional coronary model in cardiac catheterisation laboratories," *Frontiers in Cardiovascular Medicine*, vol. 11, 2024.

[39] J. Song, S. Kouidri, F. Bakir, "Numerical study on flow topology and hemodynamics in tortuous coronary artery with symmetrical and asymmetrical stenosis," *Biocybernetics and Biomedical Engineering*, vol. 41, no. 1, pp. 142–155, 2021.

[40] K. E. Hoque, S. Sawall, M. A. Hoque, M. S. Hossain, "Hemodynamic simulations to identify irregularities in coronary artery models," *Journal of Advances in Mathematics and Computer Science*, vol. 28, no. 5, pp. 1–19, 2018.

[41] M. Jahangiri, M. Saghafian, M. R. Sadeghi, "Numerical simulation of hemodynamic parameters of turbulent and pulsatile blood flow in flexible artery with single and double stenoses," *Journal of Mechanical Science and Technology*, vol. 29, no. 8, pp. 3549–3560, 2015.

[42] M. H. Amiri, A. Keshavarzi, A. Karimipour, M. Bahiraei, M. Goodarzi, J. A. Esfahani, "A three-dimensional numerical simulation of non-Newtonian blood flow through femoral artery bifurcation with a moderate arteriosclerosis: Investigating Newtonian/non-Newtonian flow and its effects on elastic vessel walls," *Heat and Mass Transfer*, vol. 55, no. 7, pp. 2037–2047, 2019.

[43] P. V. Deshpande, A. Buradi, G. N. Nagaharish, N. B. Hallad, A. Madhusudhan, B. J. Bora, "Numerical simulation of blood flow study in an idealized bifurcated coronary artery," *Fluid Mechanics and Fluid Power*, vol. 2, pp. 13–18, 2023.

[44] R. Badal, S. Jena, M. Pisupati, E. K. Kumar, V. Kumar, S. K. Panda, "Multiphysics (stress and deformation) behaviour of stented bifurcated coronary artery (soft tissue) under pulsatile flow condition," *Journal of Vibration Engineering and Technologies*, vol. 12, no. 2, pp. 1687–1694, 2024.

[45] M. Stuber, R. M. Botnar, P. G. Danias, D. K. Sodickson, K. V. Kissinger, M. Van Cauteren, et al., "Double-oblique free-breathing high resolution three-dimensional coronary magnetic resonance angiography," *Journal of the American College of Cardiology*, vol. 34, no. 2, pp. 524–531, 1999.

[46] S. H. Moon, J. H. Byun, J. W. Kim, S. H. Kim, K. N. Kim, J. J. Jung, et al., "Clinical usefulness of the angle between left main coronary artery and left anterior descending coronary artery for the evaluation of obstructive coronary artery disease," *PLoS ONE*, vol. 13, no. 9, p. e0202249, 2018.

[47] K. E. Hoque, M. Ferdows, S. Sawall, E. E. Tzirtzilakis, M. A. Xenos, "The impact of hemodynamic factors in a coronary main artery to detect the atherosclerotic severity: Single and multiple sequential stenosis cases," *Physics of Fluids*, vol. 33, no. 3, pp. 1–14, 2021.

[48] M. Andayesh, A. Shahidian, M. Ghassemi, "Numerical investigation of renal artery hemodynamics based on the physiological response to renal artery stenosis," *Biocybernetics and Biomedical Engineering*, vol. 40, no. 4, pp. 1458–1468, 2020.

[49] M. Abbasian, M. Shams, Z. Valizadeh, A. Moshfegh, A. Javadzadegan, "Effects of different non-Newtonian models on unsteady blood flow hemodynamics in patient-specific arterial models with in-vivo validation," *Computer Methods and Programs in Biomedicine*, vol. 186, p. 105185, 2020.

[50] A. A. Soares, S. Gonzaga, C. Oliveira, A. Simões, A. I. Rouboa, "Computational fluid dynamics in abdominal aorta bifurcation: Non-Newtonian versus Newtonian blood flow in a real case study," *Computer Methods in Biomechanics and Biomedical Engineering*, vol. 20, no. 8, pp. 822–831, 2017.

[51] M. Sinnott, P. W. Cleary, M. Prakash, "An investigation of pulsatile blood flow in a bifurcation artery using a grid-free method," in *Proc. 5th Int. Conf. CFD in the Process Industries*, pp. 1–6, 2006.

[52] M. Nasir, K. E. Hoque, M. M. Billah, "The impact of multiple stenosis and aneurysms on arterial diseases: A cardiovascular study," *Heliyon*, vol. 10, no. 5, p. e26889, 2024.

[53] S. Park, S. W. Lee, O. K. Lim, I. Min, M. Nguyen, Y. B. Ko, et al., "Computational modeling with fluid-structure interaction of the severe M1 stenosis before and after stenting," *Neurointervention*, vol. 8, no. 1, p. 23, 2013.

[54] L. F. U. Delestri, D. Lombardi, S. Marino, M. S. Olivieri, A. Redaelli, "Modelling of cardiac biventricular electromechanics with coronary blood flow to investigate the influence of coronary arterial motion on coronary haemodynamic," *Computer Methods and Programs in Biomedicine*, p. 108800, 2025.